Histidine–Lysine Axial Ligand Switching in a Hemoglobin: A Role for Heme Propionates

Dillon B. Nye[†], Matthew R. Preimesberger[†‖], Ananya Majumdar[‡], and Juliette T. J. Lecomte[†*]

[†] T.C. Jenkins Department of Biophysics, Johns Hopkins University, Baltimore, MD 21218, United States
[‡] Biomolecular NMR Center, Johns Hopkins University, Baltimore, Maryland, 21218, United States
[‖] Current address: Cellmig Biolabs Inc., Cambridge, MA 02142, United States

Supporting Information

Figure S1: Heme structure, nomenclature, and modification

Figure S2: Overlay of electronic absorption spectra of Fe(II) PP GlbN-A at pH 7.2 and 10.5

Figure S3: Overlay of electronic absorption spectra of PP and PPDME GlbN at neutral pH

Figure S4: Comparison of 1D ^{1}H NMR spectra of Fe(III) PP GlbN and PPDME GlbN

Figure S5: Example amide ^{1}H-^{15}N chemical shift changes in Fe(III) PPDME GlbN compared to PP GlbN

Figure S6: Example amide ^{1}H-^{15}N chemical shift changes in Fe(II) PPDME GlbN-A compared to PP GlbN-A

Figure S7: Electronic absorption spectra of Fe(III) PPDME GlbN as a function of pH

Figure S8: Upfield regions of the 1D ^{1}H NMR and ^{1}H-^{15}N HSQC spectra of Fe(II) PPDME GlbN-A showing the axial lysine NζH$_2$ group

Figure S9: Location of the lysines in the three-dimensional structure of *bis*-histidine GlbN-A

Figure S10: 1D ^{1}H NMR and electronic absorption spectra of Fe(II) PPDME K42L GlbN-A at alkaline pH

Figure S11: Upfield regions of the 1D ^{1}H NMR spectrum of Fe(II) PPDME GlbN-A at pH 9.3 and pH 10.5

Figure S12: NMR spectra of Fe(II) PPDME GlbN-A at pH 9.5 at high pressure

Figure S13: Exchange build-up curves for Lys42 signals in the ^{1}H-^{1}H EXSY experiment used for exchange rate constant determination in Fe(II) PPDME GlbN-A

Figure S14: Aromatic portion of the DQF-COSY spectrum of Fe(II) PPDME GlbN-A

Figure S15: Overlay of a portion of the ^{1}H-^{15}N HSQC and ^{1}H-N_z-^{15}N ZZ exchange spectra of Fe(II) PPDME GlbN-A at alkaline pH

Figure S16: Annotated ^{1}H-N_z-^{1}H ZZ exchange spectrum and CSP plot of Fe(II) PPDME GlbN-A at alkaline pH

Figure S17: Electronic absorption spectra showing the formation of the heme–His117 linkage in PP GlbN, PP K42L GlbN, PPDME GlbN, and PPDME K42L GlbN

Figure S18: Kinetics of formation of the heme-His117 linkage analyzed by singular value decomposition

Figure S19: 1D ^{1}H NMR and electronic absorbance spectra of Fe(II) PP H46L GlbN-A

Table S1: Heme and select side chain assignments for Fe(III) PPDME GlbN at pH 7.2, comparison to Fe(III) PP GlbN

Table S2: Heme and select side chain assignments for His–Fe–His and His–Fe–Lys conformations of Fe(II) PPDME GlbN-A at pH 9.6

Table S3: Sequence statistics for relatives of GlbN

Derivation of the pKa equation.

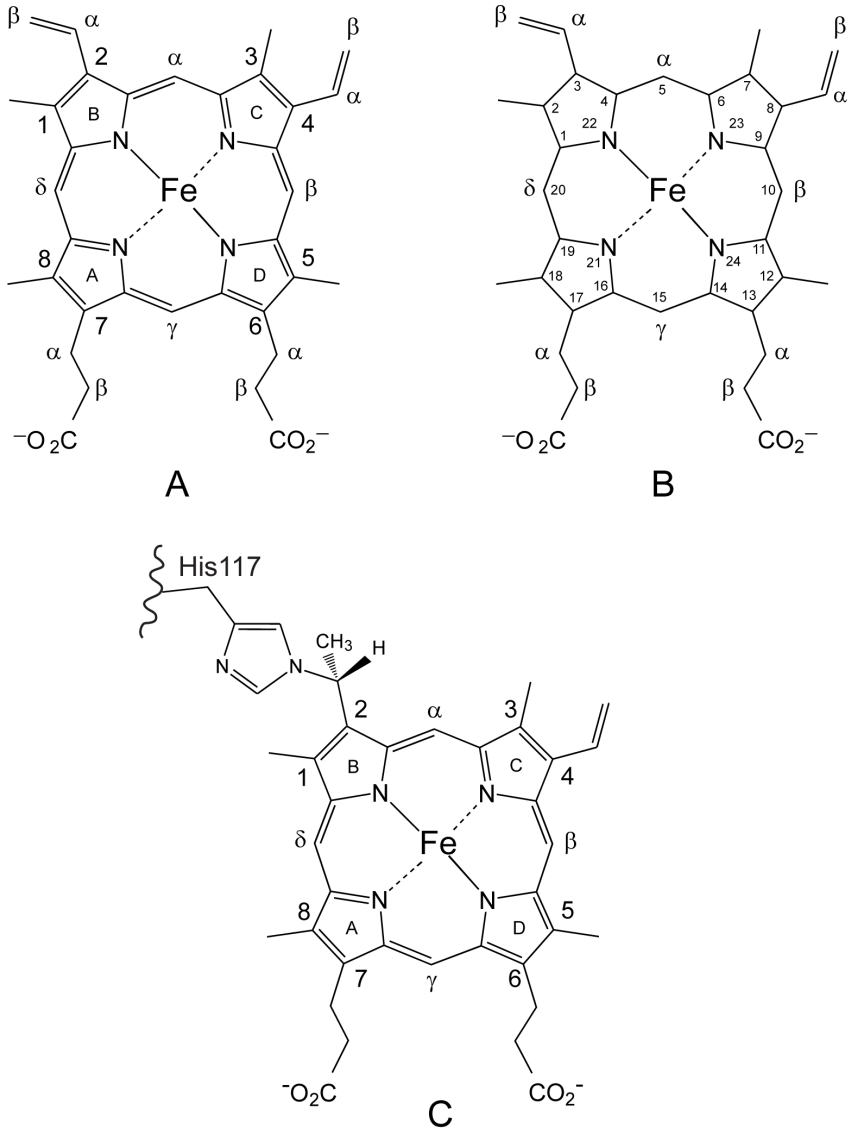

Figure S1: Heme nomenclature. (**A**) Fischer numbering used in the text. (**B**) IUPAC numbering; double bonds have been removed for clarity. The propionates on pyrroles A and D are methyl-esterified in PPDME. (**C**) The heme group after the post-translational modification.

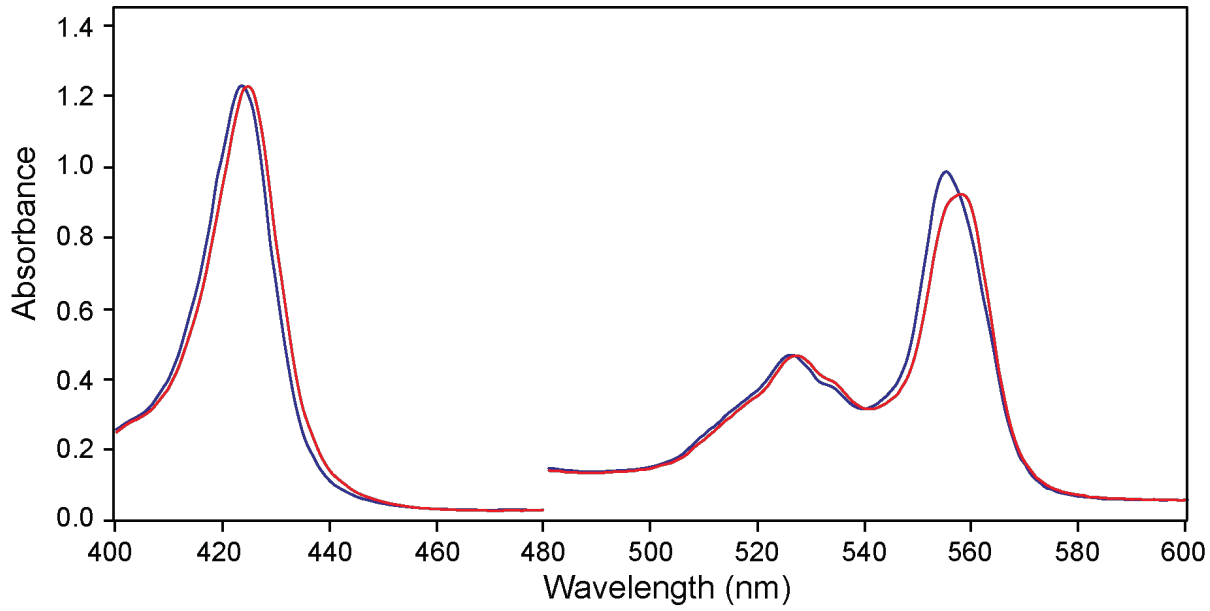

Figure S2: Electronic absorption spectra of Fe(II) PP GlbN-A at neutral pH (9 μM, 100 mM potassium phosphate, pH 7.2, red) and alkaline pH (9 μM, 100 mM sodium (bi)carbonate buffer, pH 10.5, blue). The spectra were acquired 2 min after treatment of the Fe(III) PP GlbN-A form with dithionite. The visible region has been scaled 5-fold to highlight the spectral changes at alkaline pH.

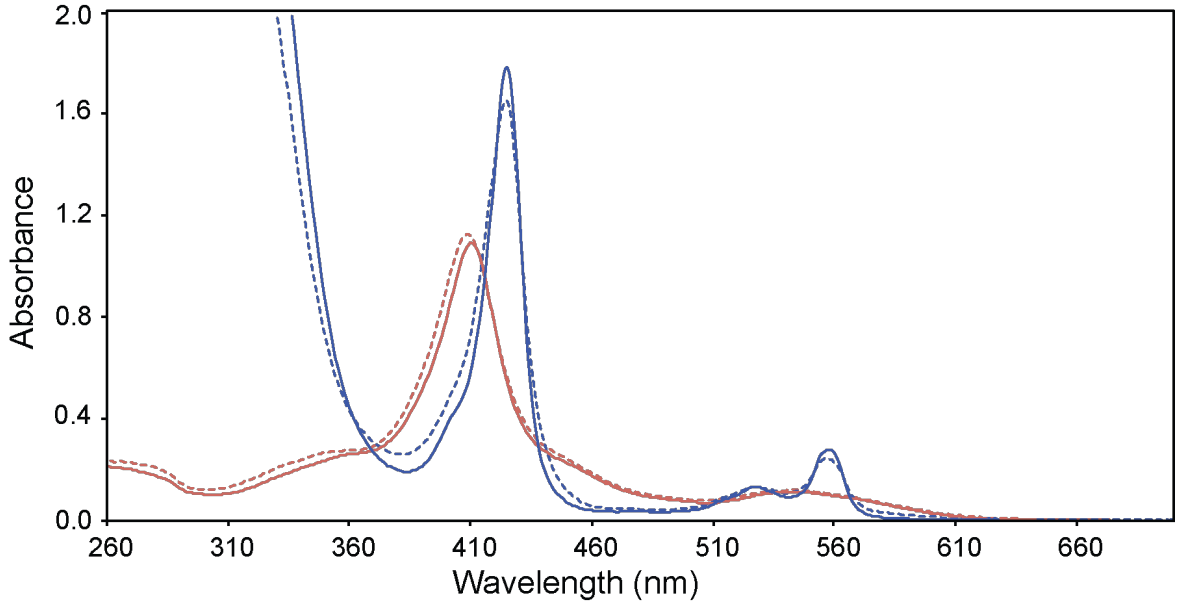

Figure S3. Electronic absorption spectra of GlbN at neutral pH (11 μM, 100 mM potassium phosphate, pH 7.2). Fe(III) PPDME GlbN (dashed red trace) was treated with dithionite and incubated for 2 min, resulting in the formation of Fe(II) PPDME GlbN-A (dashed blue trace). Also shown are the spectra of Fe(III) PP GlbN (solid red trace) and Fe(II) PP GlbN-A (solid blue trace).

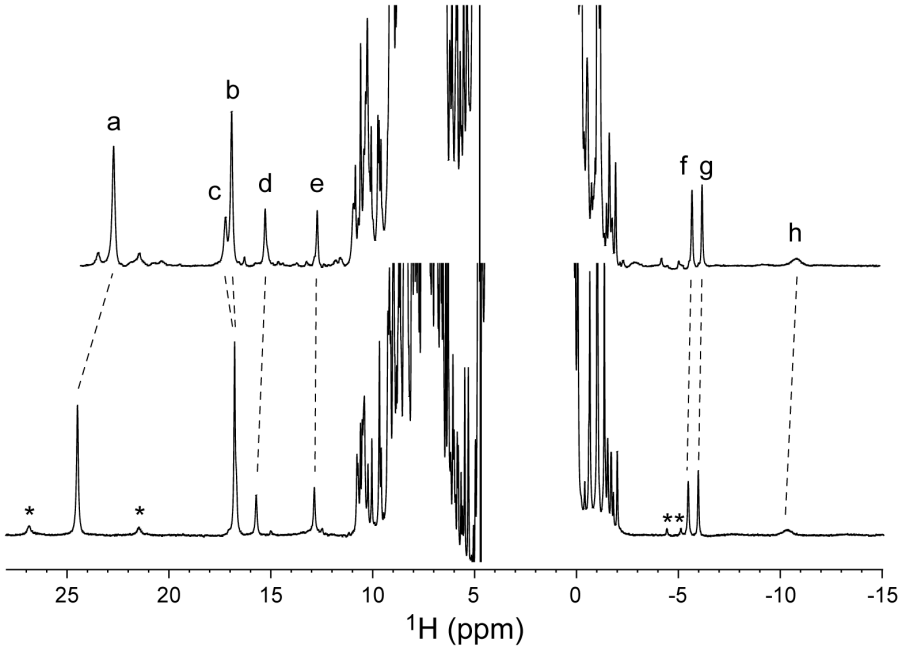

Figure S4. Comparison of the 1D ^{1}H NMR spectra of Fe(III) PPDME GlbN (top, 1.1 mM GlbN, 25 mM potassium phosphate, pH 7.2, 10% ^2H_2O, 25 °C) and Fe(III) PP GlbN (bottom, 20 mM potassium phosphate, pH 6.9). Dashed lines join signals arising from the same group in each complex. Assignments in Fe(III) PPDME GlbN were derived from those in Fe(III) PP GlbN[1] and confirmed with standard 2D ^{1}H-^{1}H experiments (see text). The resolved, annotated peaks are: a, heme 5-CH_3; b, heme 1-CH_3; c, heme 2-vinyl Hα; d, His70 Hδ1; e, His46 Hδ1; f, heme 2-vinyl $H\beta_{cis}$; g, heme 2-vinyl $H\beta_{trans}$; h, axial histidine imidazole Hε1 (or Hδ2). Small peaks such as those marked by asterisks are due to a small population of holoprotein with the heme flipped with respect to the α,γ meso axis.

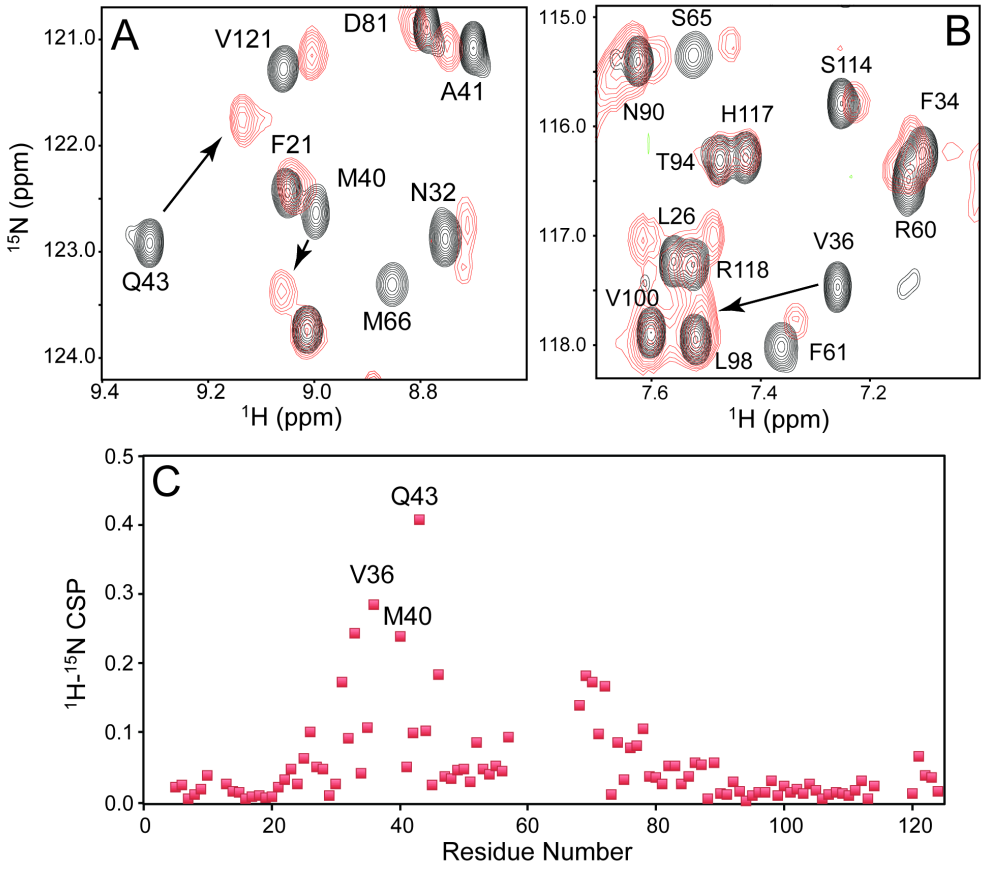

Figure S5. Comparison of amide chemical shifts of Fe(III) PPDME GlbN and Fe(III) PP GlbN at neutral pH. (**A**) and (**B**) show portions of the ^{1}H-^{15}N HSQC spectra of PP GlbN[2] (black, pH 7.3) and PPDME GlbN (red, 0.4 mM GlbN, 95 mM potassium phosphate, pH 7.0, 5% $^{2}H_2O$, 25 °C) emphasizing the CSPs for Val36, Met40, and Gln43. Marked assignments correspond to the GlbN (black) spectrum. (**C**) Plot of CSP vs. residue number for the assigned resonances of PPDME GlbN (103 of the 122 non-proline residues). The CSP is calculated from the difference in ^{1}H and ^{15}N chemical shift in PPDME GlbN compared to PP GlbN (see Materials and Methods). Significant changes are observed in the E and F helices, which provide the distal and proximal heme ligands, respectively. Resonances arising from the EF loop (residues 57–67) could not be confidently assigned in PPDME GlbN. The N-terminal portion of the E helix (residues 40–46) and the C helix (residues 31–36) show the greatest changes in chemical shift. Select heme and side chain assignments are given in Table S1.

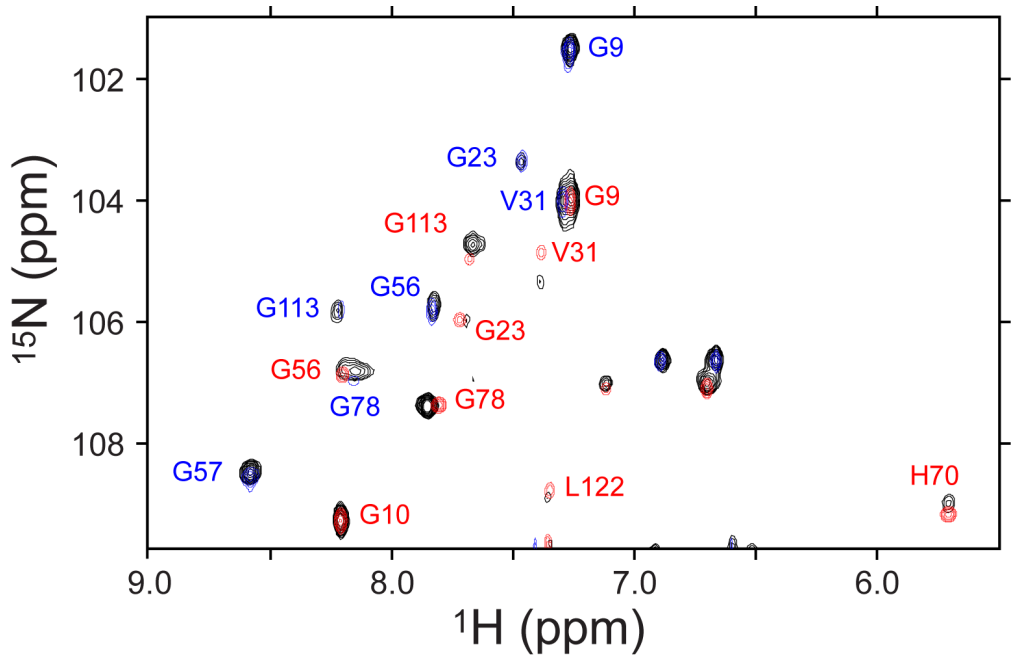

Figure S6. Comparison of the upfield (^{15}N) region of the ^{1}H-^{15}N HSQC spectrum of Fe(II) PPDME GlbN-A (black, 0.4 mM GlbN, 100 mM potassium phosphate buffer pH 7.2, 10% $^{2}H_2O$, 25 °C) with the spectrum of Fe(II) PP GlbN-A (red, pH 7.2) and the GlbN apoprotein (blue, pH 7.4). The published assignments for Fe(II) PP GlbN-A[2] and the apoprotein[3] are given in red and blue, respectively. The spectrum of Fe(II) PPDME GlbN-A is essentially a superposition of the spectra of Fe(II) PP GlbN-A and the apoprotein. This particular sample had a high level of residual apoprotein.

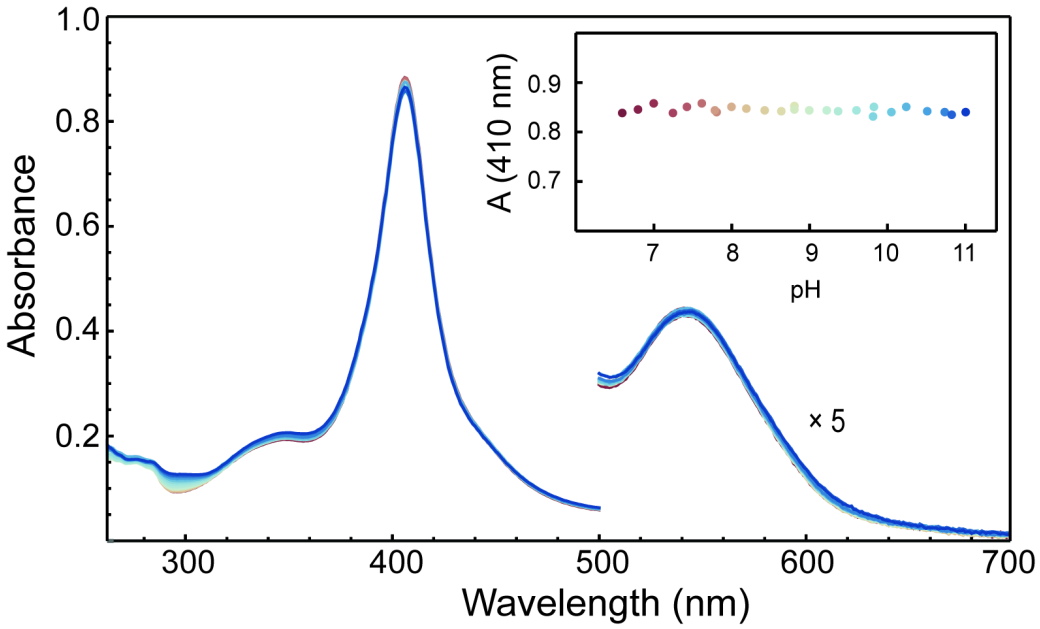

Figure S7. pH titration of Fe(III) PPDME GlbN-A monitored by electronic absorption spectroscopy. Each trace corresponds to an individual sample of ferric protein. The inset shows the pH dependence of the absorbance at 410 nm (the Soret peak maximum). The Q bands (500–700 nm, absorbance values multiplied by five) also change minimally over the pH range 6.6 to 11.2. The most significant pH-dependent changes are observed in the near-UV region of the spectrum and attributed to tyrosinate formation at alkaline pH. The data contain random error resulting from dilution correction.

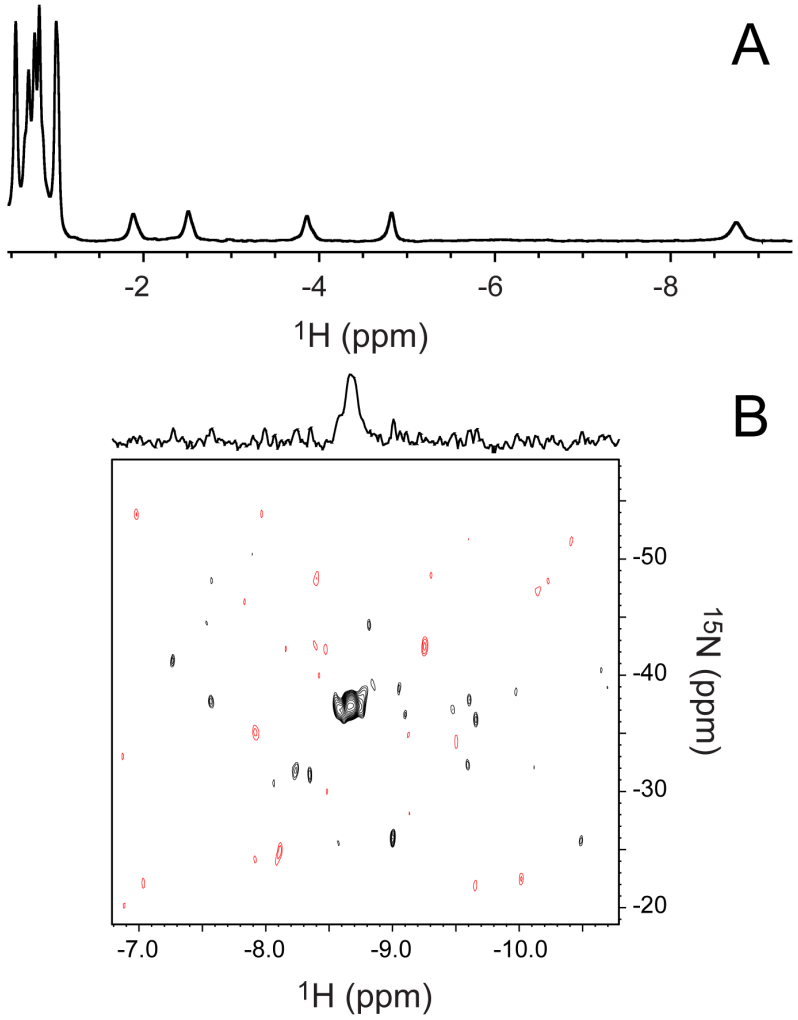

Figure S8. (**A**) The upfield portion of the 1D ^{1}H spectrum of Fe(II) PPDME GlbN-A in H_2O (~1.5 mM GlbN-A, 95 mM sodium borate buffer pH 9.7, 5% $^{2}H_2O$, 25 °C) acquired using a flipback-WATERGATE solvent suppression scheme. The far upfield peak at –8.7 ppm exchanges with solvent and is attenuated when the water signal is saturated. (**B**) The tailored ^{1}H-^{15}N HSQC spectrum of uniformly ^{15}N labeled Fe(II) PPDME GlbN-A (~700 µM GlbN, 250 mM sodium borate buffer pH 9.2, 10% $^{2}H_2O$, 25 °C). The ^{15}N carrier frequency was –35 ppm and the transfer delays were set to 3.2 ms (1/4 J for J ~ 65 Hz as expected for a lysine NH_2 group). Allowing the ^{1}H-^{15}N coupling to evolve during ^{15}N frequency labeling returned a triplet and confirmed that the ^{15}N nucleus belongs to an NH_2 spin system (data not shown).

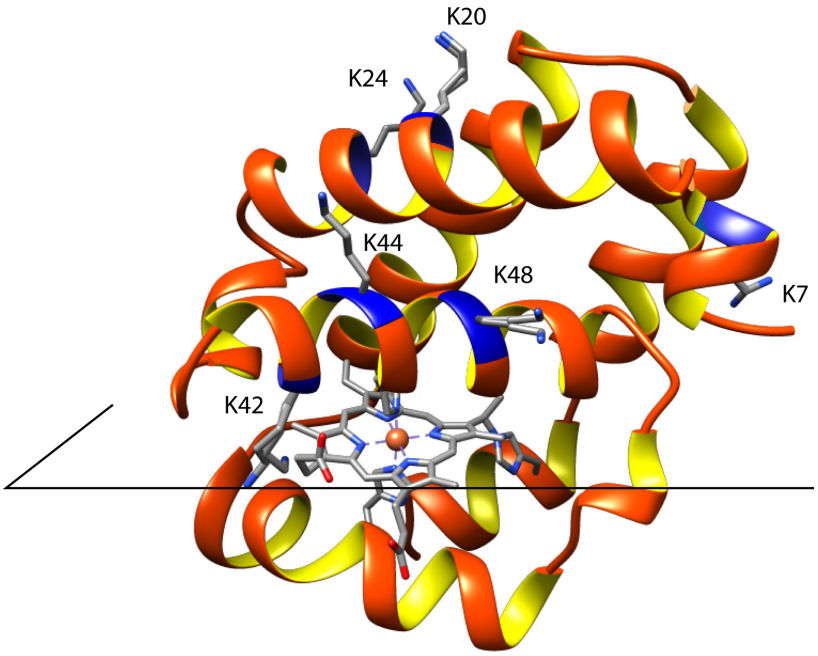

Figure S9. Location of the lysine residues in the structure of GlbN-A (PDB ID 4MAX). The outline represents the plane of the heme and divides the structure in a proximal half (below plane) and distal half (above the plane). K7, K20, K42, and K48 have more than one conformation in the crystal.

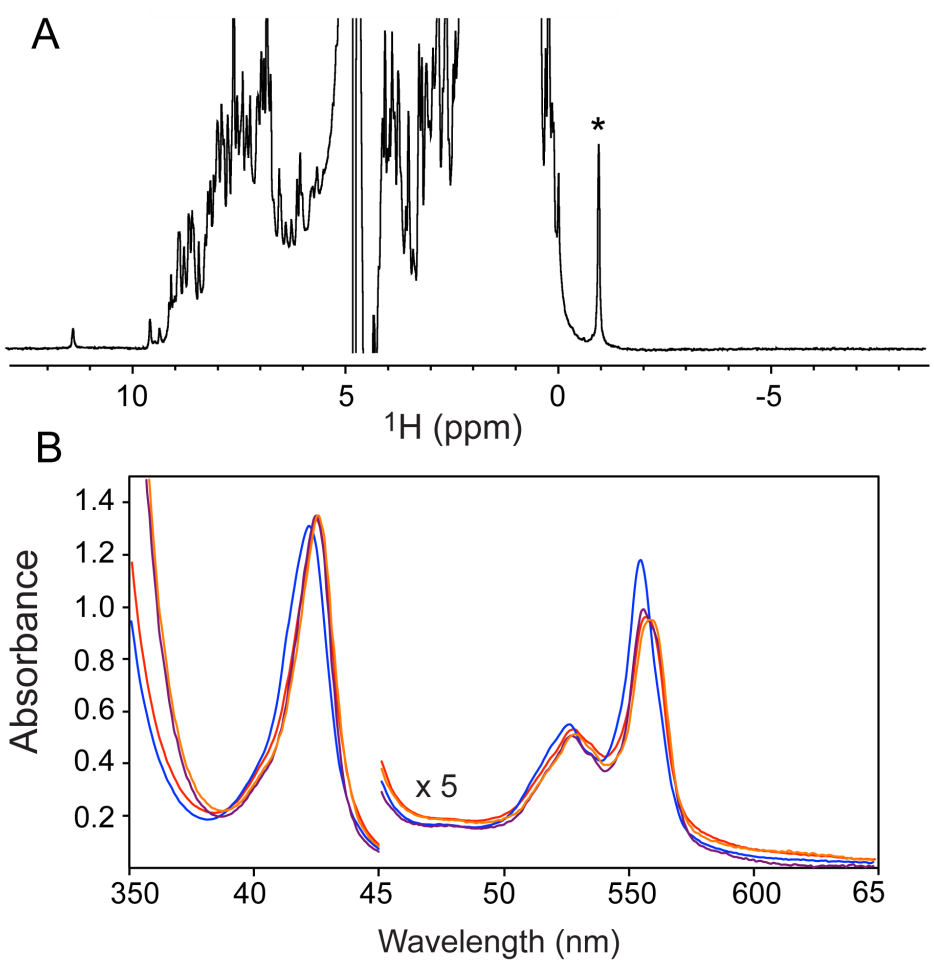

Figure S10. (**A**) The 1D ^{1}H NMR spectrum of Fe(II) PPDME K42L GlbN-A (~250 µM GlbN-A, 90 mM sodium borate buffer pH 9.2, 10% ^2H_2O, 25 °C) acquired using water presaturation. Note the complete absence of upfield peaks corresponding to a lysine heme ligand (see Figure 4 and Figure S8). The large peak at −1 ppm denoted with an asterisk corresponds to the overlapping CH_3 groups of Val121 (see Figure 4). (**B**) The electronic absorption spectra of Fe(II) PPDME K42L GlbN-A at pH 7.0 (orange, ~4 µM GlbN-A, 100 mM potassium phosphate buffer) and pH 9.2 (purple, ~4 µM GlbN-A, 100 mM sodium borate buffer). For comparison the spectra of Fe(II) PPDME GlbN-A at pH 7.0 (red) and pH 9.2 (blue) are reproduced from Figure 3. The K42L GlbN-A spectra were linearly scaled according to the ferric Soret absorbance (2.3 fold) for ease of comparison. Note that the spectrum of PPDME K42L GlbN-A changes minimally over this pH range.

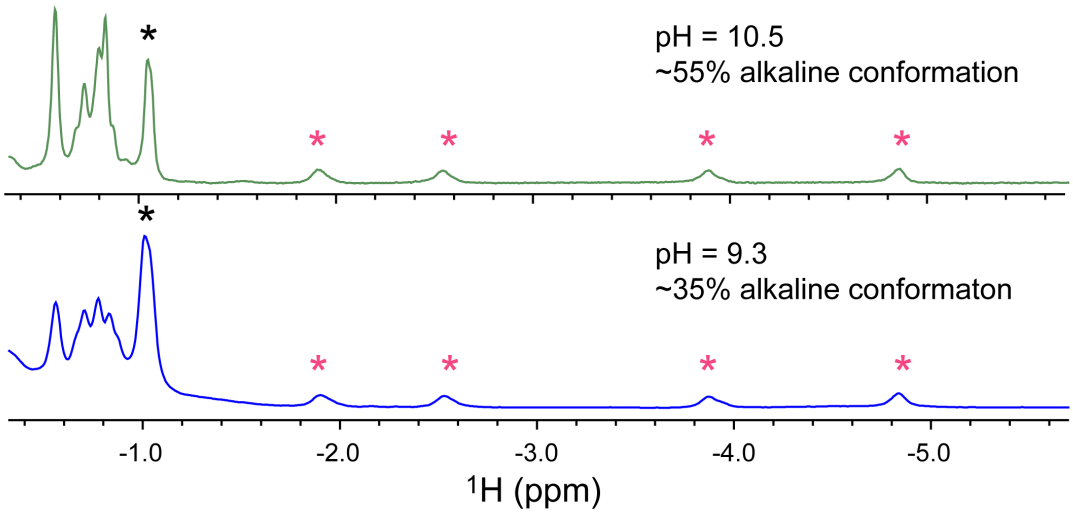

Figure S11. ^{1}H 1D NMR spectra of Fe(II) PPDME GlbN-A at pH 10.5 (0.5 mM GlbN-A, 90 mM sodium (bi)carbonate buffer, top, green) and pH 9.3 (1.3 mM GlbN-A, 90 mM sodium borate buffer, bottom, blue). The black asterisks denote the overlapping CH_3 signals of Val121 in the native His–Fe–His conformation; the red asterisks denote the Hε, Hε', Hδ and Hδ' signals of the axial lysine in the His–Fe–Lys conformation. Deconvolution of the region between –0.2 and –6.0 ppm was performed with TopSpin to obtain population estimates.

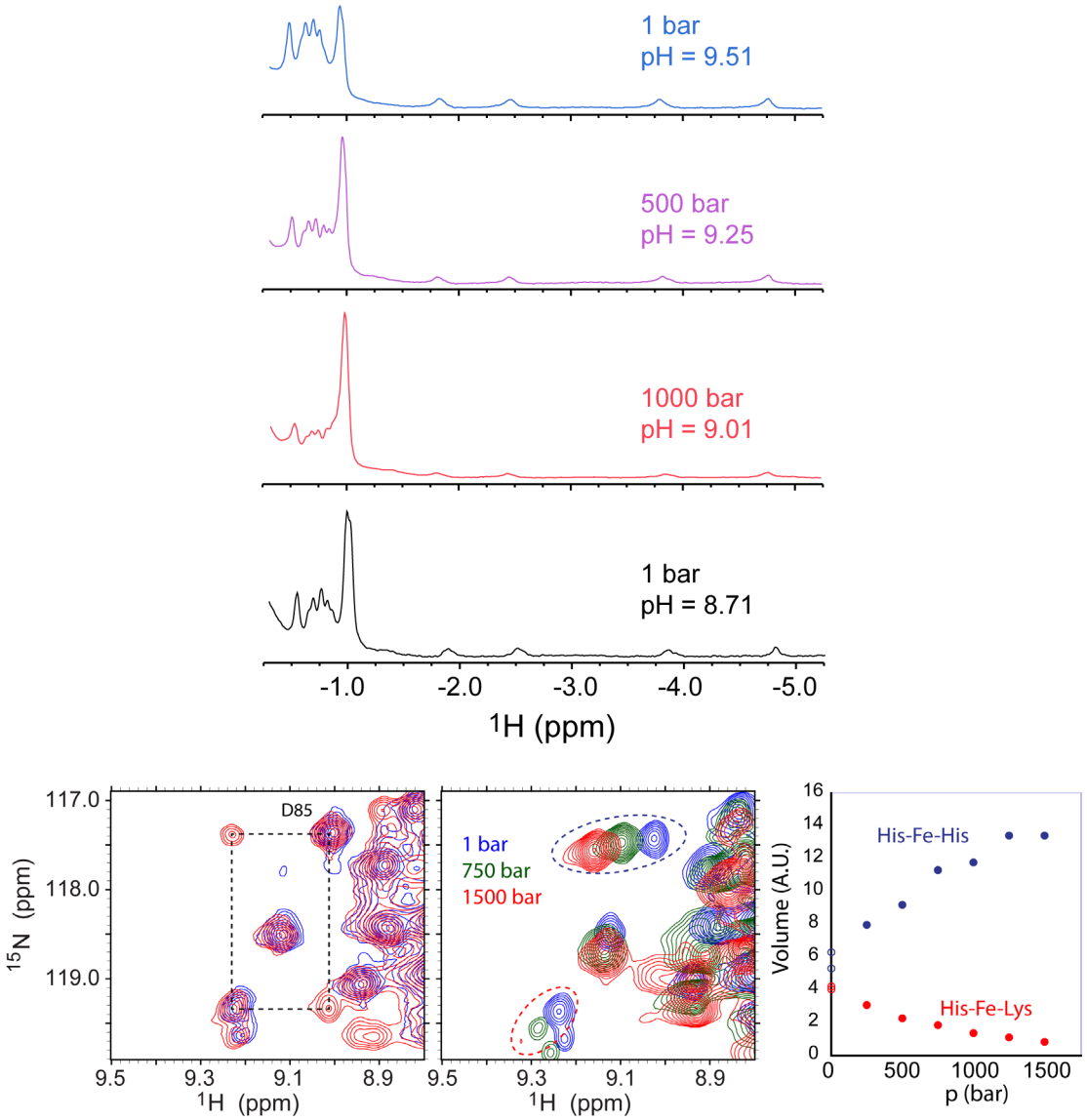

Figure S12. The response of Fe(II) PPDME GlbN-A (1 mM GlbN-A, 90 mM sodium borate buffer pH 9.51 at 1 bar, 25 °C) to hydrostatic pressure. Top: The ^{1}H NMR spectra acquired at 1 bar (blue, pH 9.51), 500 bar (purple, pH 9.25) and 1000 bar (red, pH 9.01) are shown. The solution pH at high pressure is calculated from the known pressure dependence of the ionization of boric acid.[4] The spectral changes induced by pressure were found to be fully reversible. The spectrum of Fe(II) PPDME GlbN-A (black, 0.2 mM GlbN-A, 90 mM sodium borate buffer pH 8.71, 10% $^{2}H_2O$, 1 bar, 25 °C) is shown for comparison. Note the weakening of the peaks attributed to the axial Lys42 while the signals from the His–Fe–His species increase. Bottom: Left, identification of D85 amide cross peak in the His–Fe–Lys state via ^{1}H-N_z-^{15}N ZZ exchange data; Center, pressure response of the ^{1}H-^{15}N HSQC spectrum; Right: disappearance of the His–Fe–Lys state as pressure is increased.

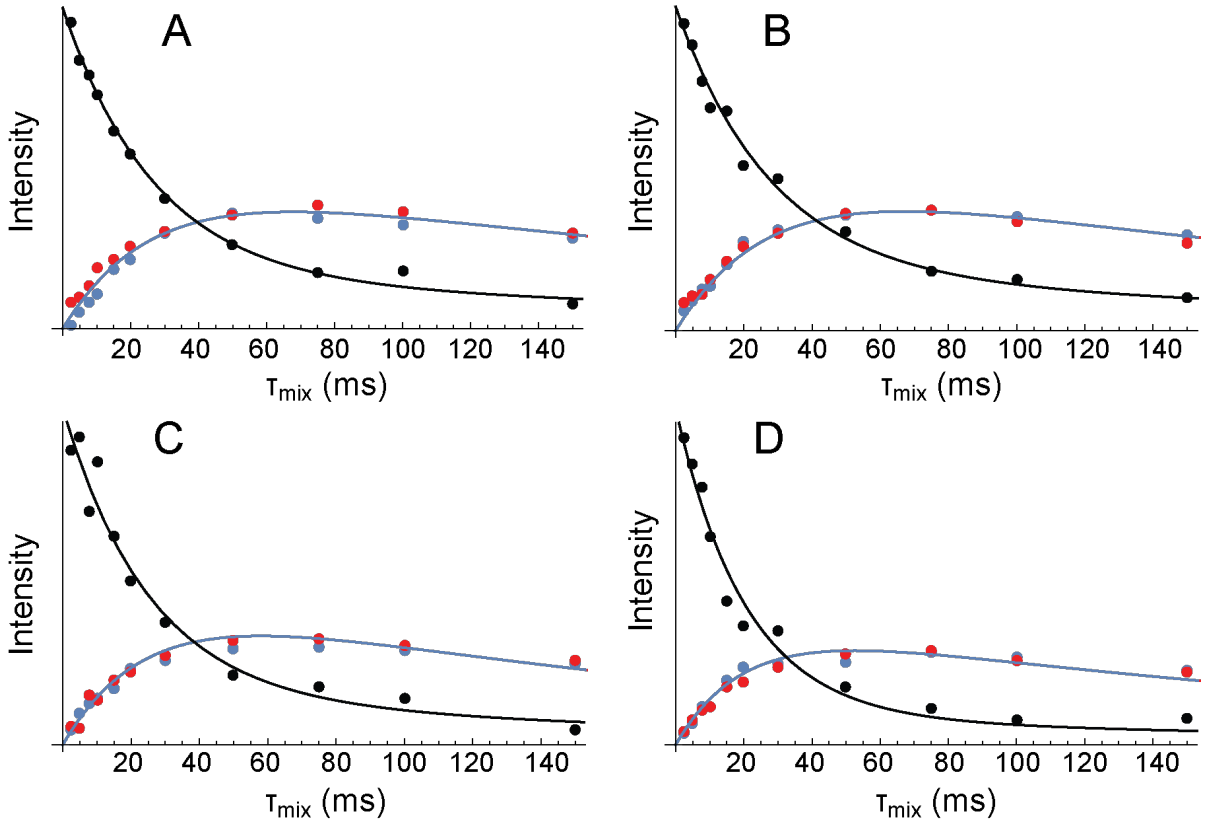

Figure S13. The exchange spectroscopy curves for Lys42 signals in Fe(II) PPDME GlbN-A (1.7 mM GlbN-A, 90 mM sodium borate buffer pH 9.3, 10% ^2H_2O, 25 °C). Intensities of self and cross peaks are plotted against the longitudinal exchange mixing time. Each panel corresponds to an individual resonance of Lys42: (**A)** Hε, –4.8 ppm; (**B**) Hδ, –3.9 ppm; (**C**) Hε', –2.1 ppm; (**D**) Hδ', –1.9 ppm. Black: diagonal peaks in His–Fe–Lys conformation; blue, exchange cross peak from the His–Fe–Lys to the His–Fe–His conformation; red, exchange cross peak from the His–Fe–His conformation to the His–Fe–Lys conformation. The solid lines represent a global fit to the standard equations describing longitudinal exchange. The initial intensities and longitudinal relaxation constants of the His–Fe–His diagonal peaks could not be determined because these peaks are not resolved. The fits were therefore used only to determine the initial intensity of the His–Fe–Lys diagonal peaks and verify the soundness of the data rather than extract parameters. Resolved ^1H resonances in the 1D spectrum were used to determine the ratio of the two conformations in this sample (see Figure S11). The ratio of exchange peak intensity to initial intensity at short mixing times (τ_{mix} = 2.5, 5.0, 7.5, and 10.0 ms) yielded the first-order rate constants of chemical exchange by linear fit. The numbers reported in the text are averages.

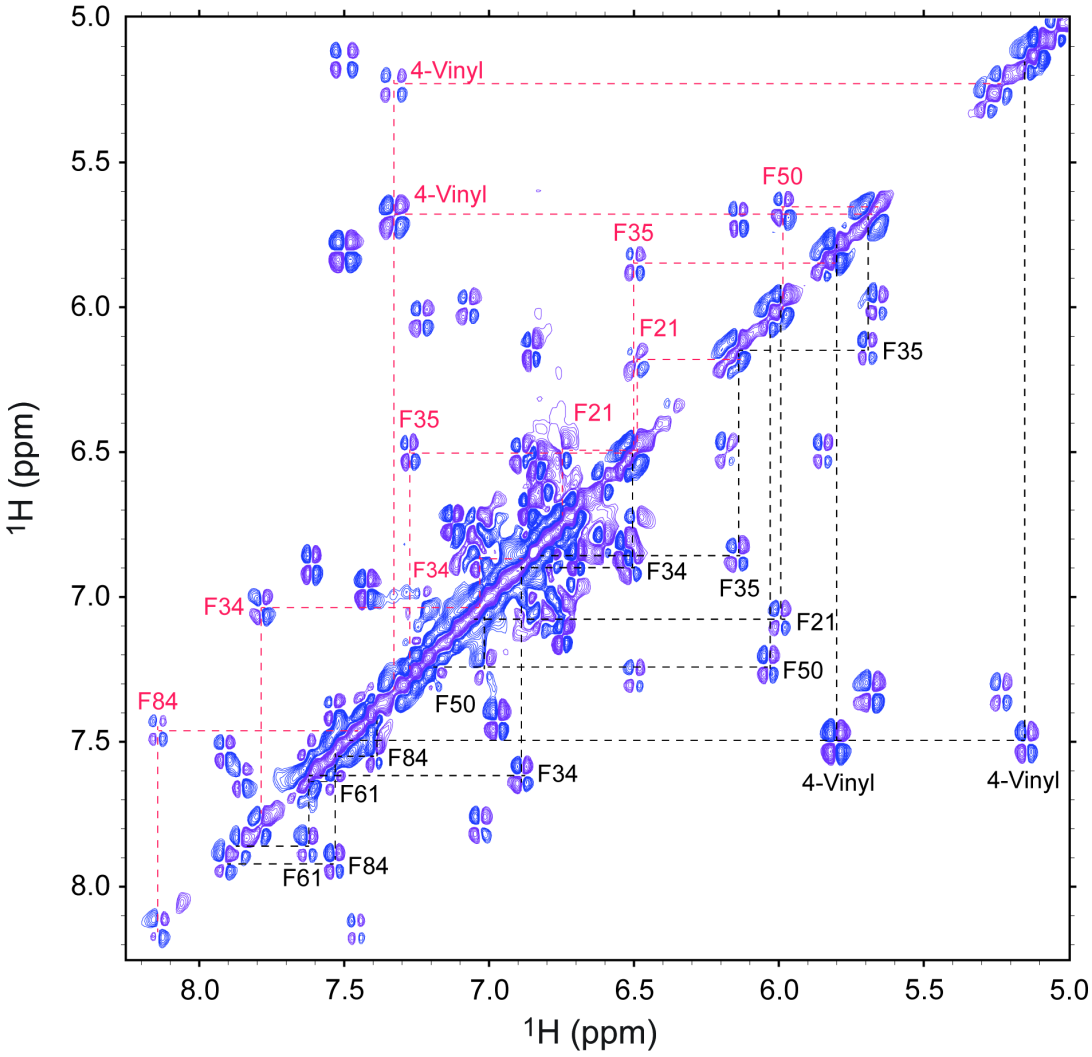

Figure S14. Aromatic region of the DQF-COSY spectrum collected on Fe(II) PPDME GlbN-A (1.5 mM GlbN-A, 100 mM sodium borate pH* 9.7, 99% ^2H_2O, 17 °C). Assignments for the native conformation are given in black below the diagonal while those for the alkaline conformation are given in red above the diagonal. The dashed lines connect the spin systems: Hδ,δ'H, Hε,ε' and Hζ of F21, F34, F35, F50, F61, and F84, and the αH and βH_2 of the heme 4-vinyl group. The COSY spectrum is free from cross peaks arising from chemical exchange, unlike the ^{1}H-^{1}H NOESY and TOCSY spectra. Chemical shifts are listed in Table S2.

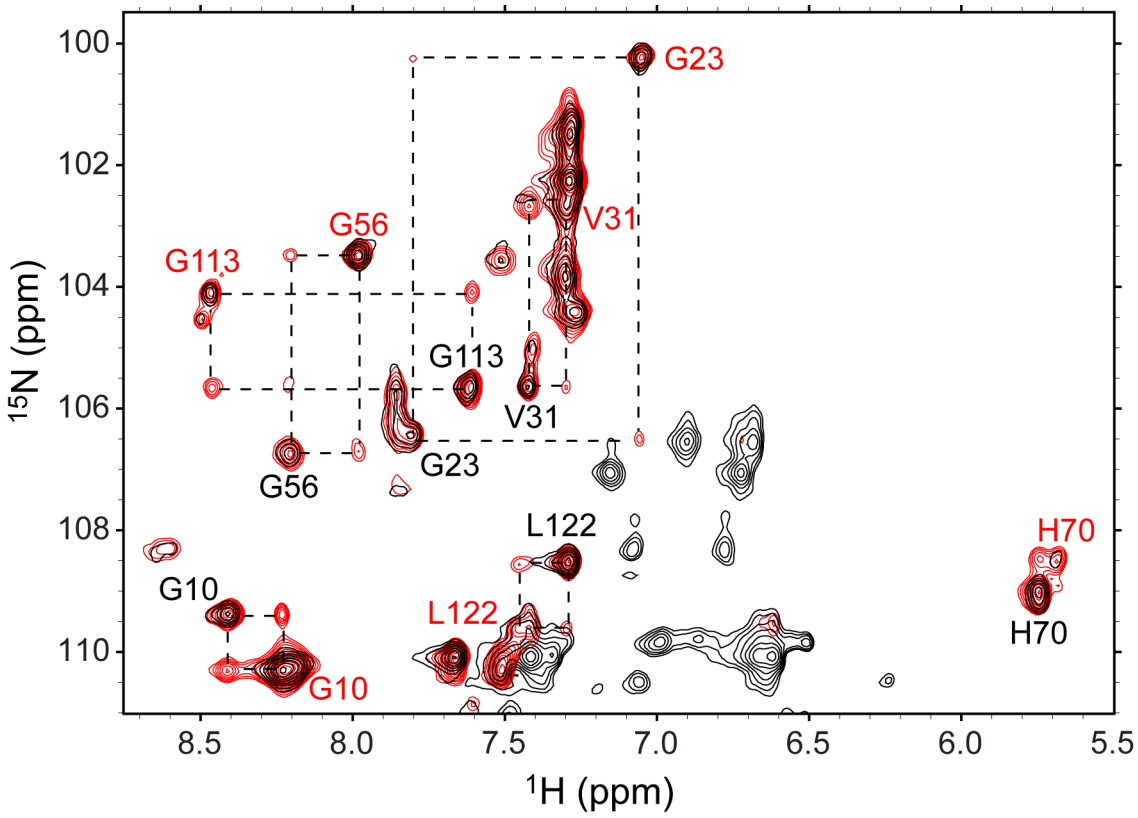

Figure S15. The glycine region of the ^{1}H-^{15}N HSQC (black) and ^{1}H-N_z-^{15}N ZZ exchange (red, τ_{mix} = 50 ms) spectra of Fe(II) PPDME GlbN-A (0.5 mM GlbN-A, 90 mM sodium borate buffer pH 9.8, 10% $^{2}H_2O$, 25 °C). Dashed lines connect exchange correlated peaks with His–Fe–His assignments in black font and His–Fe–Lys assignments in red font.

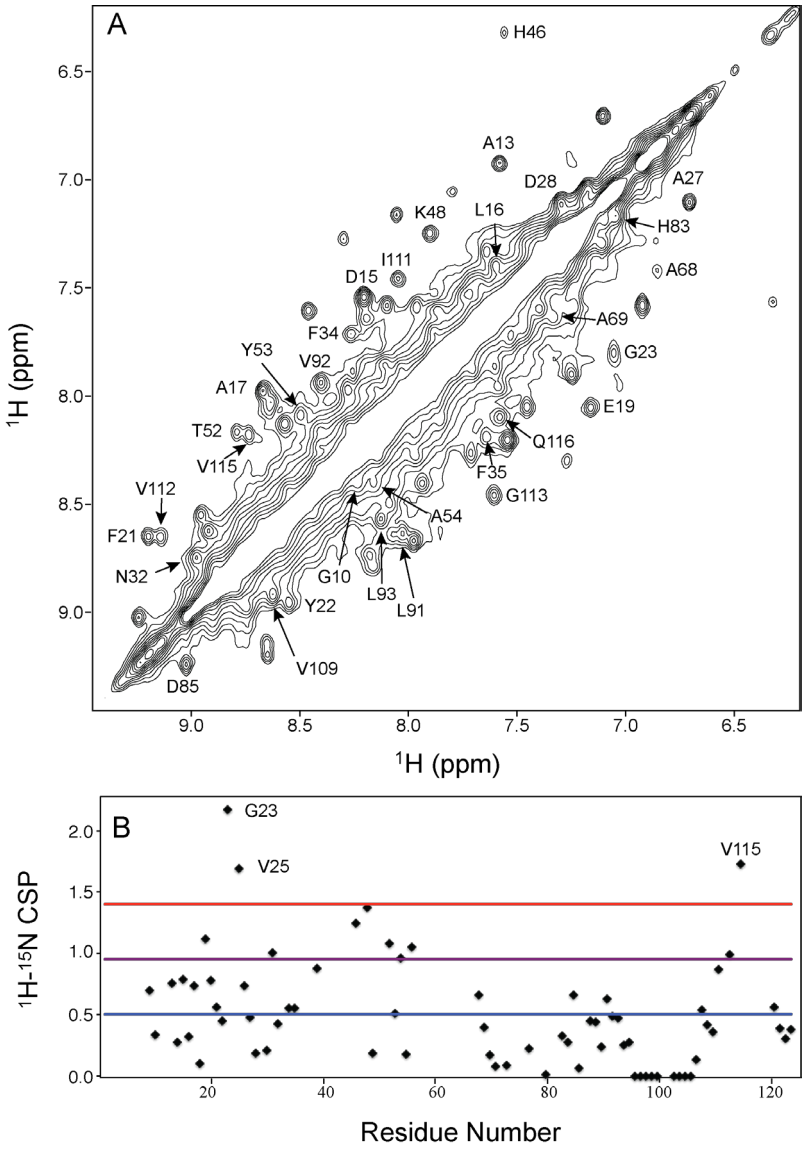

Figure S16. Chemical shift difference between the His–Fe–His and His–Fe–Lys conformations of Fe(II) PPDME GlbN-A. (**A**) The ^{1}H-^{15}N$_z$-^{1}H ZZ exchange spectrum of Fe(II) PPDME GlbN-A (0.5 mM GlbN-A, 100 mM sodium borate buffer, pH 9.8, 10% ^{2}H$_2$O, 25 °C). Resolved peaks are labeled according to assignments determined by ^{1}H-^{15}N-^{1}H NOESY-HSQC on the same sample and transferred from published His–Fe–His assignments at pH 7.2.[2] (**B**) A plot of the CSP determined for the 70 amides that could be assigned in both conformations. Lines are drawn to represent the average (blue) and standard deviation (purple for +1 SD, red for +2 SD) of the CSPs. See also Figure 8.

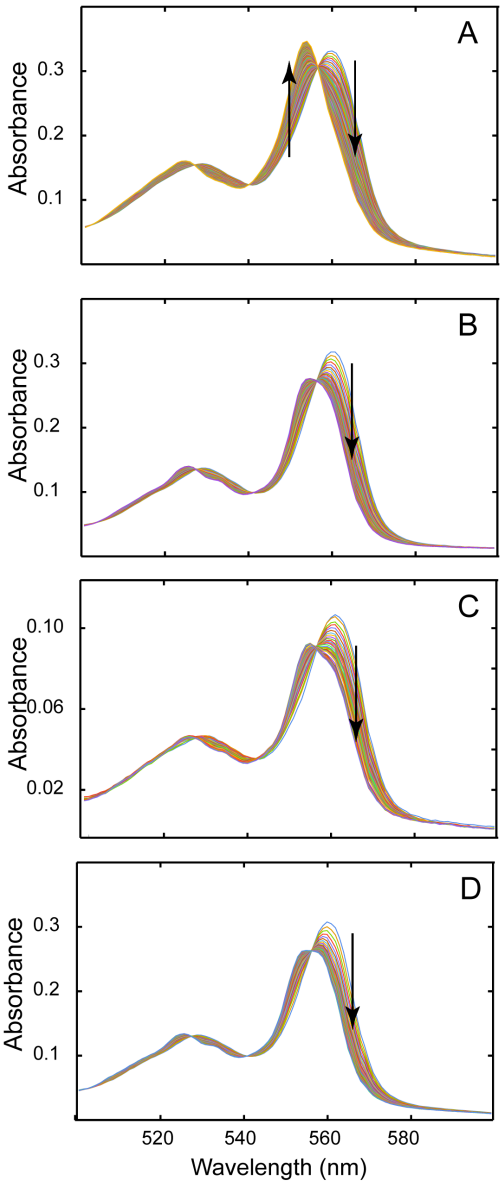

Figure S17. Formation, monitored by electronic absorption, of the heme–His117 crosslink in PPDME GlbN (**A**), PP GlbN (**B**), PPDME K42L GlbN (**C**), and PP K42L GlbN (**D**) in 100 mM sodium borate buffer pH 9.2. The black arrows denote the time progression.

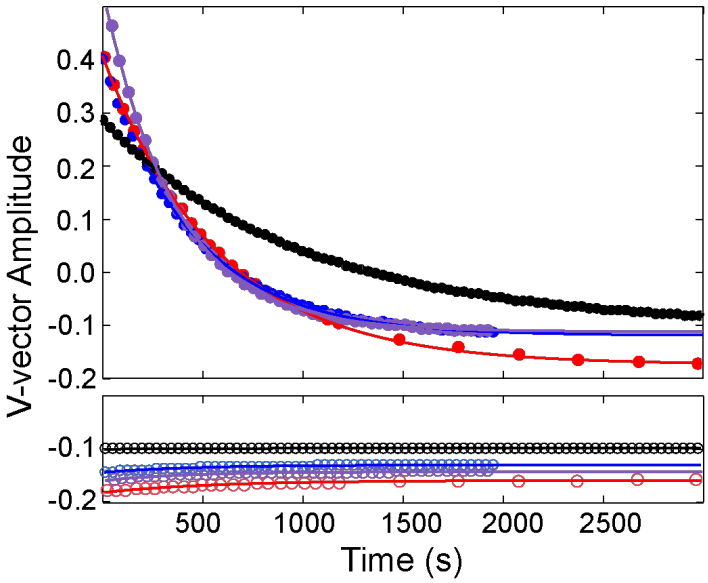

Figure S18. Kinetics of PTM in PP GlbN (blue), PPDME GlbN (black), PP K42L GlbN (purple) and PPDME K42L GlbN (red). The first (open circles) and second (closed circles) V-vectors from the SVD analysis of optical data (Figure S17) are shown. For each protein, the solid lines represent a global fit to a single exponential. The V-vectors are shown separately and the second vector for PPDME GlbN has been inverted for ease of comparison.

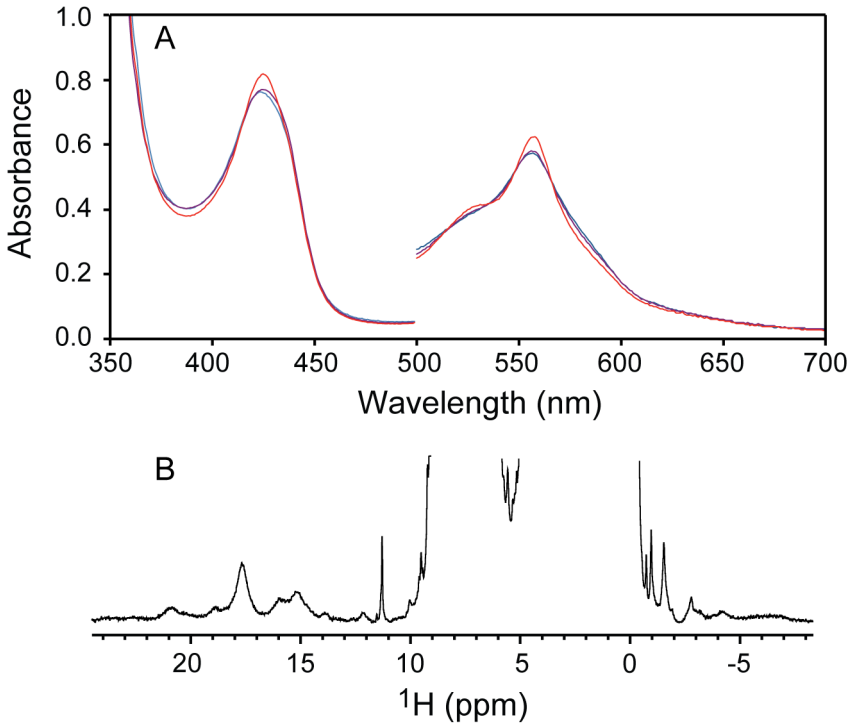

Figure S19. Optical and NMR spectra of Fe(II) PP H46L GlbN. (**A**) The absorbance spectra of Fe(II) PP H46L GlbN at pH 7.3 (blue, 100 mM potassium phosphate buffer) pH 9.3 (purple, 100 mM sodium borate buffer) and pH 10.9 (red, 100 mM sodium (bi)carbonate buffer). (**B**) The ^{1}H NMR spectrum of Fe(II) PP H46L GlbN (~0.3 mM GlbN, 90 mM sodium borate buffer pH 9.5, 10% $^{2}H_2O$, 25 °C) supporting that the protein is primarily in a high-spin pentacoordinate state at this pH.

Table S1. Heme and select side chain ^{1}H assignments in Fe(III) PPDME GlbN and comparison to Fe(III) PP GlbN

	PPDME GlbN[1]	PP GlbN[2]
Heme 1-methyl	16.93	16.52
Heme 3-methyl	7.45	7.51
Heme 5-methyl	22.76	24.27
Heme 8-methyl	8.99	9.70
Heme 2-vinyl (α, β_{cis}, β_{trans})	17.24, –6.16, –5.67	16.45, –5.80, –5.31
Heme 4-vinyl (α, β_{cis}, β_{trans})	5.34, –1.91, –1.61	5.46, –1.96, –1.67
Heme 6-substituent (α, α', β, β', ε)	10.97, 10.24, 2.11, 1.86, N.D.	11.22, 8.62, 1.24, 0.52, N.A.
Heme 7-substituent (α, α', β, β', ε)	2.72, 1.45, –0.26, –0.51, 0.04	2.15, 1.57, –0.78, –1.22, N.A.
Heme δ-meso	–0.02	0.09
Phe21 ($\delta\delta$', $\varepsilon\varepsilon$', ζ)	7.34, 7.81, 6.70	7.39, 7.83, 6.72
Val25 (α, β, γ1, γ2)	3.24, 1.97, 0.56, 0.41	3.29, 2.05, 0.66, 0.56
Phe34 ($\delta\delta$', $\varepsilon\varepsilon$', ζ)	6.37, 6.12, 5.85	6.35, 6.11, 5.74
Phe35 ($\delta\delta$', $\varepsilon\varepsilon$', ζ)	7.68, 8.34, 6.12	7.84, 8.76, 6.97
His46 (α, β, β', δ1)	7.85, 10.44, 9.11, 12.74	7.99, 10.81, 9.23, 12.93
Phe50 ($\delta\delta$', $\varepsilon\varepsilon$', ζ)	5.38, 5.56, 5.91	5.29, 5.54, 5.91
Phe61 ($\delta\delta$', $\varepsilon\varepsilon$', ζ)	6.52, 6.46, 6.83	6.45, 6.35, 6.69
Ala69 (α, β)	3.82, 0.06	3.94, 0.31
His70 (α, β, β', δ1)	7.53, 10.36, 9.20, 15.29	7.50, 10.44, 9.26, 15.75
Leu73 (α, γ, δ1, δ2)	4.16, 1.96, 0.41, –0.21	4.08, 1.84, –0.68, 0.25
Leu79 (γ, δ1, δ2)	0.87, –1.15, 0.44	0.80, –1.28, 0.29
Phe84 ($\delta\delta$', $\varepsilon\varepsilon$', ζ)	6.48, 7.00, 6.86	6.52, 7.06, 6.94
Ile87 (α, β, γ1, γ1', γ2, δ)	3.13, 0.22, –0.01, –0.05, –0.98, –1.05	3.16, 0.22, –0.01, –0.03, –0.97, –0.97
Val121 (α, β, γ1, γ2)	6.85, 3.07, 3.21, 2.66	6.93, 3.14, 3.31, 2.76

N.D., not determined; N.A., not applicable

[1]25 mM potassium phosphate buffer pH 7.2, 10% $^{2}H_2O$, 25 °C.

[2]Based on published assignments.[1]

Table S2. Heme and select side chain ^{1}H assignments in Fe(II) PPDME GlbN-A[1]

	His–Fe–His state	His–Fe–Lys state
Heme 1-methyl	2.55	3.14
Heme 3-methyl	3.27	3.31
Heme 5-methyl	2.63	3.48
Heme 8-methyl	3.54	2.89
Heme 2-ethyl (α, β)	6.34, 0.98	6.73, 2.53
Heme 4-vinyl (α, β_{cis}, β_{trans})	7.50, 5.15, 5.81	7.33, 5.23, 5.69
Heme α-meso	8.87	8.92
Heme β-meso	8.68	9.10
Heme γ-meso	9.10	8.69
Heme δ-meso	8.91	9.22
Phe21 (δδ', εε', ζ)	6.83, 7.07, 6.00	6.75, 6.50, 6.19
Val25 (α, β, γ1, γ2)	3.13, 1.30, –0.03, 0.15	3.39, 0.94, –0.77, –0.48
Phe34 (δδ', εε', ζ)	7.62, 6.89, 6.51	7.78, 7.03, 6.87
Phe35 (δδ', εε', ζ)	6.86, 6.14, 5.69	7.27, 6.50, 5.85
Lys42 (α, β,β', γ, γ', δ, δ', ε, ε', ζ)	N.D., N.D., N.D., N.D., N.D., 1.80, 1.80, 3.13, 3.13, N.D.	4.44, 0.47, 1.06, –0.82, –0.25, –3.82, –1.81, –4.78, –2.44, –8.75[2]
His46 (δ2, ε1)	0.55, 1.59	7.65, 8.12
Phe50 (δδ', εε', ζ)	6.04, 7.23, 7.02	5.66, 5.67, 5.99
Phe84 (δδ', εε', ζ)	7.40, 7.53, 7.91	7.40, 7.46, 8.15
His117 (δ2, ε1)	7.04, 7.00	8.49, 7.60
Val121 (α, β, γ1, γ2)	1.80, 1.20, –0.96, –0.93	1.84, 1.19, –0.70, –0.62

N.D., not determined

[1]99% $^{2}H_2O$, pH* 9.7, 17 °C.

[2]10% $^{2}H_2O$, pH 9.7, 17 °C.

Table S3. Occupancy of selected sites in 341 GlbN relatives (see Materials and Methods)

Residue and position	number	percentage
His at 46	173	51%
Lys at 46	79	23%
Lys at 42	104	31%
Arg at 42	120	35%
His at 46 and Lys at 42	60	18%

pH Titration Analysis

We follow an approach similar to that of Nelson and Bowler (2000)[5] with two modifications. We consider the ionization of the lysine as opposed to a "trigger group" and we include the 5c species to allow for weak distal ligation as occasionally observed in hemoglobins.

$HH\|K$	His–Fe–His complex with neutral lysine
$HH\|K^+$	His–Fe–His complex with charged lysine
$HK\|H$	His–Fe–Lys complex with neutral histidine
$H\|HK$	His–Fe complex with neutral distal histidine and lysine
$H\|HK^+$	His–Fe complex with neutral distal histidine and charged lysine

$$
\begin{aligned}
HH|K \rightleftharpoons H|HK \qquad & K_1 = \frac{[H|HK]}{[HH|K]} \\
HK|H \rightleftharpoons H|HK \qquad & K_2 = \frac{[H|HK]}{[HK|H]} \\
HH|K^+ \rightleftharpoons HH|K + H^+ \qquad & K_3 = \frac{[HH|K][H^+]}{[HH|K^+]} \\
H|HK^+ \rightleftharpoons H|HK + H^+ \qquad & K_3 = \frac{[H|HK][H^+]}{[H|HK^+]} \\
& \frac{K_1}{K_2} = \frac{[HK|H]}{[HH|K]}
\end{aligned}
$$

where we assumed that the ionization of the lysine is independent of histidine coordination.

$$
\begin{aligned}
Q &= \frac{1}{[HK|H]}\left([HK|H] + [H|HK] + [HH|K] + [HH|K^+] + [H|HK^+]\right) \\
&= 1 + K_2 + \frac{K_2}{K_1} + \frac{K_2}{K_1}\frac{[H^+]}{K_3} + \frac{K_2[H^+]}{K_3} \\
f_{HK|H} &= \frac{1}{Q} \\
f_{HH|K} &= \frac{1}{Q}\frac{K_2}{K_1} \\
f_{H|HK} &= \frac{1}{Q}K_2 \\
f_{HH|K^+} &= \frac{1}{Q}\frac{K_2}{K_1}\frac{[H^+]}{K_3} \\
f_{H|HK^+} &= \frac{1}{Q}\frac{K_2[H^+]}{K_3}
\end{aligned}
$$

As an approximation, the $[H|HK]$ and $[H|HK^+]$ terms are ignored. $HH|K^+$ is spectroscopically indistinguishable from $HH|K$. Thus, at each pH value the observables report on $[HH|K^+] + [HH|K]$ and $[HK|H]$.

The apparent midpoint of the transition occurs when

$$\begin{aligned} [HH|K^+] &= [HK|H] + [HH|K] \\ f_{HH|K^+} &= f_{HK|H} + f_{HH|K} \\ \frac{K_2}{K_1}\frac{[H^+]_{1/2}}{K_3} &= 1 + \frac{K_2}{K_1} \end{aligned}$$

$$\begin{aligned} [H^+]_{1/2} &= \frac{K_1 K_3}{K_2} + \frac{K_1 K_3 K_2}{K_1 K_2} \\ &= \left(\frac{K_1}{K_2} + 1\right) K_3 \end{aligned}$$

and

$$pK(\text{app}) = -\log[H^+]_{1/2}$$

References

(1) Scott, N. L., Falzone, C. J., Vuletich, D. A., Zhao, J., Bryant, D. A., and Lecomte, J. T. J. (2002) The hemoglobin of the cyanobacterium *Synechococcus* sp. PCC 7002: Evidence for hexacoordination and covalent adduct formation in the ferric recombinant protein. *Biochemistry 41*, 6902-6910.

(2) Pond, M. P., Majumdar, A., and Lecomte, J. T. J. (2012) Influence of heme post-translational modification and distal ligation on the backbone dynamics of a monomeric hemoglobin. *Biochemistry 51*, 5733-5747.

(3) Vuletich, D. A., Falzone, C. J., and Lecomte, J. T. J. (2006) Structural and dynamic repercussions of heme binding and heme-protein cross-linking in *Synechococcus* sp. PCC 7002 hemoglobin. *Biochemistry 45*, 14075-14084.

(4) Tsuda, M., Shirotani, I., Minomura, S., and Terayama, Y. (1976) Effect of pressure on dissociation of weak acids in aqueous buffers. *B. Chem. Soc. Jpn. 49*, 2952-2955.

(5) Nelson, C. J., and Bowler, B. E. (2000) pH dependence of formation of a partially unfolded state of a Lys 73 -> His variant of iso-1-cytochrome *c*: Implications for the alkaline conformational transition of cytochrome *c*. *Biochemistry 39*, 13584-13594.